Title

CXCR7 influences leukocyte entry into the CNS parenchyma by controlling abluminal CXCL12 abundance during autoimmunity.

Journal

The Journal of experimental medicine, 208(2)

ISSN

0022-1007

Authors

Cruz-Orengo, Lillian
Holman, David W
Dorsey, Denise
et al.

Publication Date

2011-02-01

DOI

10.1084/jem.20102010

Peer reviewed

CXCR7 influences leukocyte entry into the CNS parenchyma by controlling abluminal CXCL12 abundance during autoimmunity

Lillian Cruz-Orengo,[1] David W. Holman,[1] Denise Dorsey,[1] Liang Zhou,[5,6] Penglie Zhang,[7] Melissa Wright,[1] Erin E. McCandless,[2] Jigisha R. Patel,[1] Gary D. Luker,[8,9] Dan R. Littman,[10,11] John H. Russell,[3] and Robyn S. Klein[1,2,4]

[1]Department of Internal Medicine, [2]Department of Pathology and Immunology, [3]Department of Developmental Biology, and [4]Department of Anatomy and Neurobiology, Washington University School of Medicine, St. Louis, MO 63110
[5]Department of Pathology and [6]Department of Microbiology-Immunology, Feinberg School of Medicine, Northwestern University, Chicago, IL 60611
[7]Department of Medicinal Chemistry, ChemoCentryx Inc., Mountainview, CA 94043
[8]Department of Radiology and [9]Department of Microbiology and Immunology, University of Michigan Medical School, Ann Arbor, MI 48109
[10]Department of Pathology and [11]Department of Microbiology, Skirball Institute Program of Molecular Pathogenesis, New York University, New York, NY 10016

Loss of CXCL12, a leukocyte localizing cue, from abluminal surfaces of the blood–brain barrier occurs in multiple sclerosis (MS) lesions. However, the mechanisms and consequences of reduced abluminal CXCL12 abundance remain unclear. Here, we show that activation of CXCR7, which scavenges CXCL12, is essential for leukocyte entry via endothelial barriers into the central nervous system (CNS) parenchyma during experimental autoimmune encephalomyelitis (EAE), a model for MS. CXCR7 expression on endothelial barriers increased during EAE at sites of inflammatory infiltration. Treatment with a CXCR7 antagonist ameliorated EAE, reduced leukocyte infiltration into the CNS parenchyma and parenchymal VCAM-1 expression, and increased abluminal levels of CXCL12. Interleukin 17 and interleukin 1β increased, whereas interferon-γ decreased, CXCR7 expression on and CXCL12 internalization in primary brain endothelial cells in vitro. These findings identify molecular requirements for the transvascular entry of leukocytes into the CNS and suggest that CXCR7 blockade may have therapeutic utility for the treatment of MS.

CORRESPONDENCE
Robyn S. Klein:
rklein@dom.wustl.edu

Abbreviations used: BBB, blood–brain barrier; BMEC, brain microvessel endothelial cell; CNS, central nervous system; EAE, experimental autoimmune encephalomyelitis; EGFP, enhanced GFP; ES, embryonic stem; GFAP, glial fibrillary acidic protein; GPCRs, G-protein coupled receptors; IHC, immunohistochemical; MOG, myelin oligodendrocyte glycoprotein; MS, multiple sclerosis; QPCR, quantitative RT-PCR

Multiple sclerosis (MS) is a chronic, inflammatory, and demyelinating disease of the central nervous system (CNS) characterized by the pathological infiltration of autoreactive leukocytes (Frohman et al., 2006; Man et al., 2007; McFarland and Martin, 2007). Studies examining the migratory routes of encephalitogenic T cells recently established that they invade the submeningeal CNS via perivascular scanning along transvascular pathways that originate within the meninges (Bartholomäus et al., 2009). These cells remain perivascularly localized until arriving at Virchow-Robin spaces, where access to the CNS parenchyma is accomplished via migration across astrocytic endfeet that comprise the glial limitans (Abbott et al., 2006). Restriction of leukocyte entry is thus normally accomplished via the presence of localizing cues along perivascular spaces (Körner et al., 1997; Vajkoczy et al., 2001; McCandless et al., 2006, 2008b); however, in MS this regulation is lost and cells gain inappropriate access to the CNS parenchyma. Recent data examining the blood–brain barrier (BBB) expression of CXCL12, a chemokine that restricts the CNS entry of CXCR4-expressing leukocytes (McCandless et al., 2006, 2008b), indicate that its loss from abluminal surfaces within the CNS

L. Cruz-Orengo and D.W. Holman contributed equally to this paper.

The Rockefeller University Press $30.00
J. Exp. Med. Vol. 208 No. 2 327-339
www.jem.org/cgi/doi/10.1084/jem.20102010

The Journal of Experimental Medicine

is specific to MS (McCandless et al., 2008a,b). Polarized CXCL12 expression at the BBB therefore appears to be an important component of CNS immune privilege, whereas loss of CXCL12 polarity is associated with leukocyte entry. The mechanisms responsible for altered CXCL12 expression at the CNS microvasculature are unknown; however, studies using the murine model of MS, experimental autoimmune encephalomyelitis (EAE), implicate several T cell cytokines including IL-1β, TNF, IFN-γ, and IL-17 in leukocyte entry across the CNS endothelium (Argaw et al., 2006; Afonso et al., 2007; Kebir et al., 2007; Lees et al., 2008; McCandless et al., 2009; Huppert et al., 2010), suggesting they may influence localizing cues at this site.

Recently, CXCR7 (formerly RDC-1) has been identified as an alternative receptor for CXCL12 that also binds CXCL11 (Burns et al., 2006). CXCR7 possesses homology with conversed domains of G protein–coupled receptors (GPCRs; Libert et al., 1990) and is structurally similar to other CXC receptors, although ligand binding does not initiate typical intracellular signal transduction, but instead results in β-arrestin recruitment and MAP kinase activation (Zabel et al., 2009; Rajagopal et al., 2010). CXCR7 expression studies have identified protein on the surface of B cells (Infantino et al., 2006; Sierro et al., 2007) and transcripts within the heart, kidney, and spleen (Burns et al., 2006) and in the adult CNS, within hippocampal neurons and extensively along the microvasculature (Schönemeier et al., 2008a). Studies in zebrafish development and in in vitro mammalian systems suggest CXCR7 functions primarily to sequester CXCL12 (Boldajipour et al., 2008; Mahabaleshwar et al., 2008; Naumann et al., 2010), thereby regulating signaling through CXCR4. No studies, however, have explored in vivo roles for CXCL12 sequestration within mammals in either physiological or diseased states. The coexpression of this chemokine/receptor pair at the CNS microvasculature suggests a potential mechanism for regulating CXCL12 localization along abluminal surfaces, and therefore immune privilege at the BBB.

In this study, we provide the first report of the role of CXCR7 in an in vivo disease model and provide insight into the mechanism of CXCL12 internalization at the BBB. We examined the expression and activity of CXCR7 in CNS tissues, using both in vivo and in vitro model systems. The results described here demonstrate that CXCR7 is critical in mediating CXCL12 internalization at CNS endothelial barriers in the autoimmune model EAE. In vivo antagonism of CXCR7 inhibited induction of EAE in a dose-dependent manner, while ameliorating ongoing disease. Compared with vehicle-treated animals, mice treated with CXCR7 antagonist were found to have decreased parenchymal and perivascular infiltrates, with accumulation of immune cells within the subarachnoid space, adjacent to meningeal vessels. Vehicle-treated mice with EAE showed attenuated abluminal CXCL12 expression, whereas EAE mice treated with high doses of antagonist retained perivascular CXCL12 expression pattern. Studies evaluating the impact of T cell cytokines on CXCR7-mediated sequestration of CXCL12 into lysosomal compartments determined that IL-17 and IFN-γ exhibit antagonistic effects on this process via regulation of CXCR7 expression at the mRNA level. CXCR7 appears to play an essential role in controlling abluminal expression of CXCL12, which is necessary to prevent pathological entry of immune cells into the CNS parenchyma, and is therefore an attractive pharmacologic target for therapeutic treatment of MS.

RESULTS

CXCR7 is expressed exclusively by the CNS vasculature during CNS autoimmunity

In prior studies, we observed that CXCL12 internalization within CNS postcapillary venules occurred specifically in specimens derived from individuals with CNS autoimmune disease (McCandless et al., 2006, 2008a). Given the recent discovery that CXCR7 mediates CXCL12 internalization within mammalian cells (Naumann et al., 2010), we analyzed spinal cord tissues of mice in which one copy of the CXCR7 gene was replaced with cDNA encoding enhanced GFP (EGFP; $CXCR7^{GFP/+}$). In the mutated locus, the *EGFP* gene replaces the entire open reading frame encoding exon 2 in CXCR7 (Fig. S1). GFP expression in naive $CXCR7^{GFP/+}$ mice was observed throughout the meninges and microvasculature (Fig. 1, a and b) and was increased at postcapillary venules during EAE induced by adoptive transfer of myelin oligodendrocyte glycoprotein (MOG)–specific T cells (Fig. 1, c–e). GFP colocalized with CD31 in specimens from both naive mice and from those with EAE (Fig. 1, f and g). Inflammatory infiltrates were completely devoid of GFP expression (Fig. 1, c-e, h) even after amplification with anti-GFP antibodies (Fig. 1, g and h). Analyses of mean numbers of GFP^+ venules (Fig. 1 i) and levels of GFP expression (Fig. 1 j) within white matter regions of $CXCR7^{GFP/+}$ mice revealed increases in spinal cord ($P = 0.04$) tissues, but not cerebellar and brainstem tissues, of mice with adoptive transfer EAE compared with naive animals. Baseline numbers of GFP^+ venules in the brainstem, however, were significantly higher than in the spinal cord ($P = 0.0062$), reflecting the long known increased vascularity of gray matter areas within the CNS (Craigie, 1920). Flow cytometric analysis of GFP levels within leukocytes derived from secondary lymphoid tissues of MOG-immunized wild-type and $CXCR7^{GFP/+}$ detected GFP within a small population of $CD19^+$ cells, but not in $CD4^+$, $CD8^+$, $CD11b^+$, or $CD11c^+$ cells (Fig. 1 k). Approximately 11 and 4% of $CD19^+$ cells exhibited GFP expression in splenic and lymph node tissues, respectively, of MOG-immunized mice (Fig. 1 l). No GFP expression was observed in any leukocytes in unimmunized mice (not depicted). Collectively, these data suggest that CXCR7 is expressed at endothelial cell barriers within the CNS and that this expression is increased in EAE at sites of inflammatory infiltration.

CXCR7 antagonism ameliorates EAE and decreases leukocyte entry into the CNS parenchyma

Given the predominance of CXCR7 expression on the CNS vasculature and its increase in the setting of CNS autoimmune

disease, we hypothesized that CXCR7 would impact on the localization of infiltrating immune cells via loss of CXCL12 as a localizing cue within perivascular locations. Accordingly, disruption of this process might allow abluminal CXCL12 to persist, preventing perivascular leukocytes from gaining access to the CNS parenchyma. To test this, we administered various doses of a small molecule inhibitor of CXCR7, CCX771, daily to mice beginning at the time of adoptive transfer of 10^7 MOG-specific $CD4^+$ T cells and continued throughout the course of clinical disease. CCX771 exhibits high affinity for human and mouse CXCR7 (11 nM; Zabel et al., 2009) and is completely selective relative to all other chemokine, chemotactic, and nonchemokine GPCRs tested (>10 µM; Tables S1 and S2). Subcutaneous, daily administration of CCX771 at the doses used in our studies results in high systemic exposure with a serum half-life of 6 h (Fig. S2 a) and efficient penetration into the CNS, as determined by LC-MS (Carbajal et al., 2010). Administration of CCX771 at doses of 5, 10, and 30 mg/kg led to a dose-dependent decrease in clinical disease severity (Fig. 2 a) and weight loss (Fig. 2 b) compared with animals treated with vehicle alone beginning at the time of adoptive transfer. Disease expression in adoptively transferred animals treated with vehicle was no different from similarly transferred animals that remained untreated (not depicted). The mean maximal disease severity scores of all groups of CCX771-treated versus vehicle-treated were also significantly lower ($P < 0.001$) and differences in disease and weight loss curves between groups of animals treated with 10 and 30 mg/kg doses of CCX771 were also significant ($P < 0.001$; Fig. 2, b and c).

Given that the CXCR7 antagonist CCX771 reduced clinical disease severity when administered at the time of adoptive transfer of MOG-specific T cells, we wondered whether CXCR7 antagonism could treat ongoing EAE. Thus, we compared treatment with vehicle alone with treatment with vehicle until day 9 after transfer, when animals have attained a score of 1, and then began treatment with 10 mg/kg of CCX771. We found that CCX771 significantly reduced the clinical severity of peak disease and improved the recovery of diseased animals compared with vehicle-treated

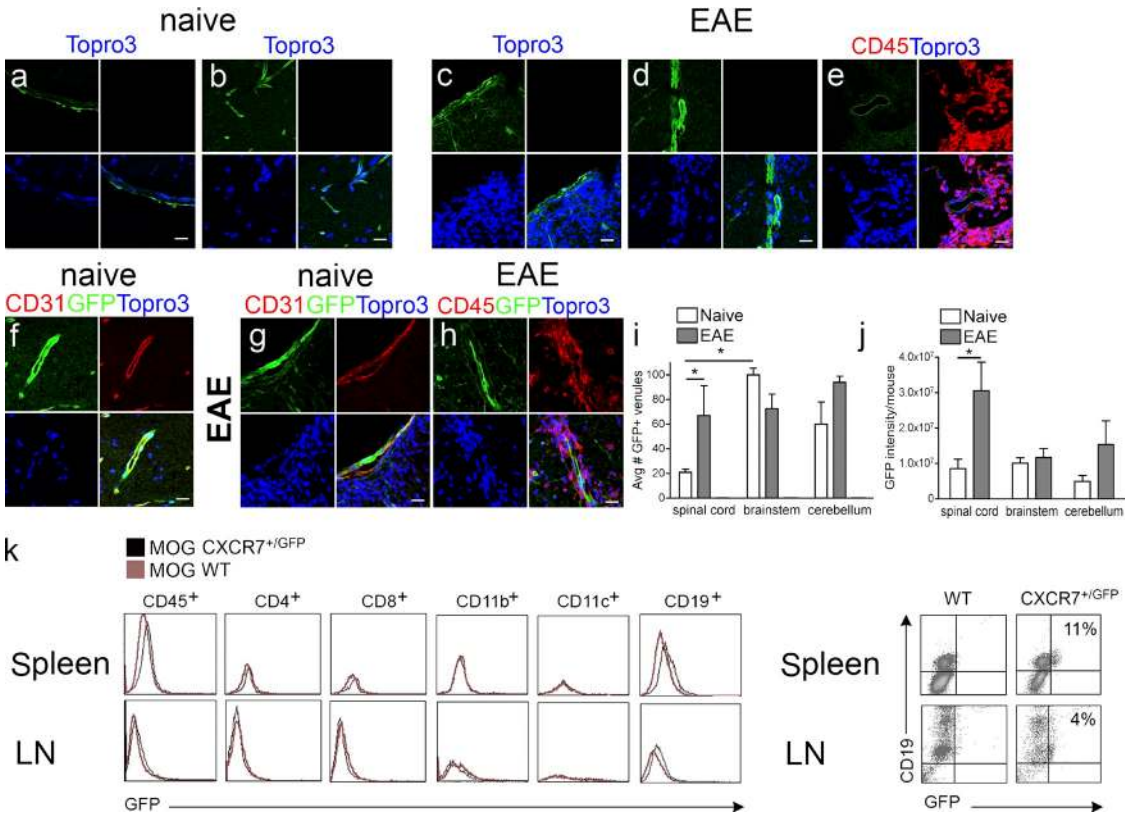

Figure 1. CXCR7 is expressed by endothelial cells within the CNS and B cells within lymphoid tissues. Spinal cord sections derived from naive $CXCR7^{GFP/+}$ mice (a, b, and f) and from those with EAE (c–e, g, and h) were evaluated via confocal microscopy for GFP fluorescence alone (green; a–d) or with expression of CD45 (red; e) and, after amplification with anti-GFP antibodies, in conjunction with detection of CD31 (f and g) and CD45 (h). All nuclei are counterstained with ToPro3 (blue). Bars, 25 µm. Quantitation of mean numbers of GFP^+ venules (i) and mean GFP levels (j) in spinal cord (SC), brainstem (BS), and cerebella (CB) of naive or EAE $CXCR7^{GFP/+}$ mice are shown. Data are expressed as the mean intensity per vessel for $n = 12$ images taken from 3 mice/group. *, $P < 0.01$. Flow cytometric analysis of expression of GFP and leukocyte markers in cells derived from spleens (top) and lymph nodes (LNs, bottom) of MOG-immunized wild-type (red lines) and $CXCR7^{GFP/+}$ (black lines) mice (k). (l) Spleen and LN cells were stained with indicated antibodies; numbers indicate percentages of $CD19^+$ cells expression GFP. Data are representative of two experiments with three mice per group.

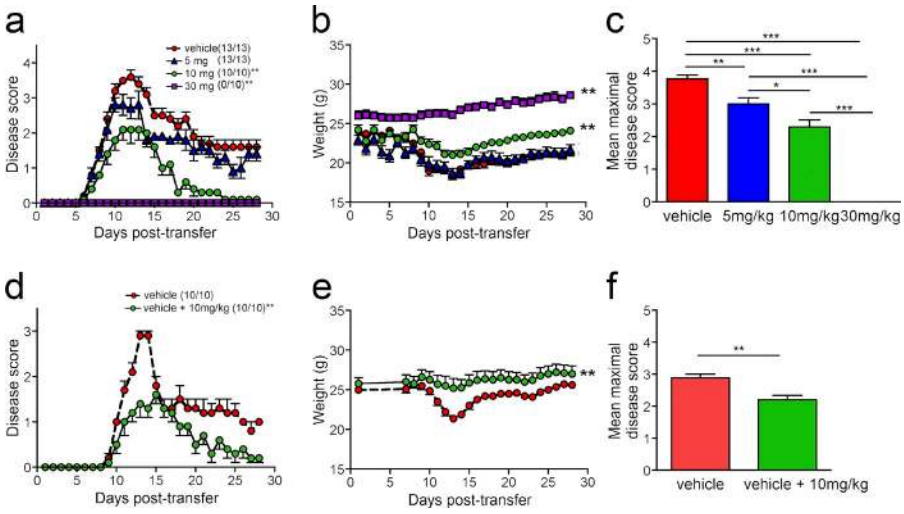

Figure 2. CXCR7 antagonism decreases the clinical severity of EAE. Mice were intravenously injected with 10×10^6 MOG-specific $CD4^+$ T cells, and dose response effects of CCX771 on disease induction (a–c) and treatment of ongoing disease (d–f) were examined. For dose-response curves evaluating clinical disease severity and weight loss (a and b), animals were grouped into those receiving vehicle or CCX771 at indicated doses daily, beginning at the time of adoptive transfer of MOG-specific $CD4^+$ T cells. Mice were monitored daily, weighed, and graded on a scale of 0–5, as described previously (McCandless et al., 2009). Numbers in parentheses indicated number of mice with disease compared with total mice in each group. Results are expressed as mean disease scores ± SEM, and curves were analyzed using one-way ANOVA compared with vehicle–treated mice. **, $P < 0.001$. (c) Mean maximal disease severity scores for animals treated with vehicle or CCX771 at indicated doses. *, $P < 0.05$; **, $P < 0.01$; ***, $P < 0.001$. To determine whether CCX771 ameliorates ongoing EAE and weight loss (d and e), animals were grouped into those receiving vehicle or vehicle until animals reached a score of 1 and then CCX771 at 10 mg/kg. Results are expressed as mean disease scores ± SEM and analyzed via one-way ANOVA. **, $P < 0.001$. (f) Mean maximal disease severity scores for animals treated with vehicle or with vehicle until development of disease and then CCX771 at 10 mg/kg. **, $P < 0.01$. Data are representative of five experiments with $n = 10–13$ animals per group.

animals, even if CCX771 treatment began when all animals had reached a score of 1 ($P = 0.0146$; Fig. 2 d). Analysis of weight loss in both groups also revealed a significant difference between vehicle and the antagonist treated groups ($P < 0.001$; Fig. 2 e), as did analysis of mean maximal disease severity scores (Fig. 2 f). These data strongly implicate CXCR7 as a disease-modifying molecule.

CXCR7 antagonism prevents leukocyte entry at the microvasculature

To examine the basis of our clinical findings, we analyzed spinal cord tissues from animals with EAE that had undergone no treatment, treatment with vehicle or with various doses of CCX771. Histological examination of spinal cord sections from vehicle- and CCX771-treated (10 mg/kg) mice with EAE at the peak of their relative disease curves (12 d after transfer), revealed dramatic differences in the extent of meningeal and parenchymal inflammatory white matter lesions, whereas animals treated with high dose CCX771 (30 mg/kg) exhibited no meningeal or parenchymal infiltrates (Fig. 3 a). Similarly, luxol fast blue (LFB) analysis of spinal cord tissues revealed decreased demyelination in mice treated with 10 or 30 mg/kg of CCX771 compared with vehicle-treated animals (Fig. S2 b). To assess the differences in meningeal inflammation between treatment groups, we used the astrocyte activation marker glial fibrillary acidic protein (GFAP) to delineate the edge of the parenchyma.

Immunohistochemical (IHC) detection of VCAM-1 and GFAP in mice treated with vehicle versus CCX771 during adoptive transfer of MOG-specific T cells revealed that mice treated with 10 mg/kg CCX771 exhibited marked increases in numbers of cell localized to the meninges compared with vehicle-treated mice and to mice treated with 30 mg/kg CCX771, which did not exhibit any meningeal inflammation (Fig. 3 b). In addition, detection of VCAM-1 and GFAP in mice treated with vehicle versus CCX771, regardless of dose, revealed meningeal VCAM-1 expression in all animals, but no parenchymal VCAM-1 expression in mice that received antagonist, despite similar levels of $GFAP^+$ expression in all mice (Fig. 3 b). Analysis of the overall width of meningeal infiltrates in 10 consecutive images under high power magnification revealed significant increases in mice treated with 10 or 5 mg/kg CCX771 versus mice treated with vehicle or left untreated ($P = 0.0003$ and 0.0243, respectively; Fig. 3 c). Quantitative assessment of the numbers of perivascular cuffs (designated as "lesions") per 10 consecutive high power fields in each section revealed significantly fewer lesions in mice treated with CCX771 at 10 mg/kg versus nontreated or vehicle-treated mice ($P = 0.0114$; Fig. 3 d). Analysis of numbers of leukocytes within perivascular cuffs observed in spinal sections from all treatment groups showed that CXCR7 antagonism led to significantly fewer lesions with extensive cuffing ($P = 0.0021$, score 2; $P = 0.0142$, score 3; Fig. 3 e).

IHC identification of subsets of infiltrating leukocytes revealed many $CD3^+$ and $CD11b^+$ cells within the meninges of mice with EAE treated with vehicle or with 10 mg/kg of CCX771, whereas mice treated with 30 mg/kg of CCX771 exhibited almost no $CD3^+$ and $CD11b^+$ cells at this location (Fig. 4 a). Few $B220^+$ cells were observed within the meninges of either vehicle or CCX771-treated animals (Fig. 4 a). Although vehicle-treated mice exhibited infiltration of $CD3^+$ and $CD11b^+$ cells within the parenchyma, mice treated with 10 mg/kg CXCR7 antagonist exhibited predominantly $CD11b^+$ cell parenchymal infiltration, whereas both $CD3^+$ and $B220^+$ cells accumulated within the meninges (Fig. 4 a). Analysis of leukocyte subsets within deep white matter

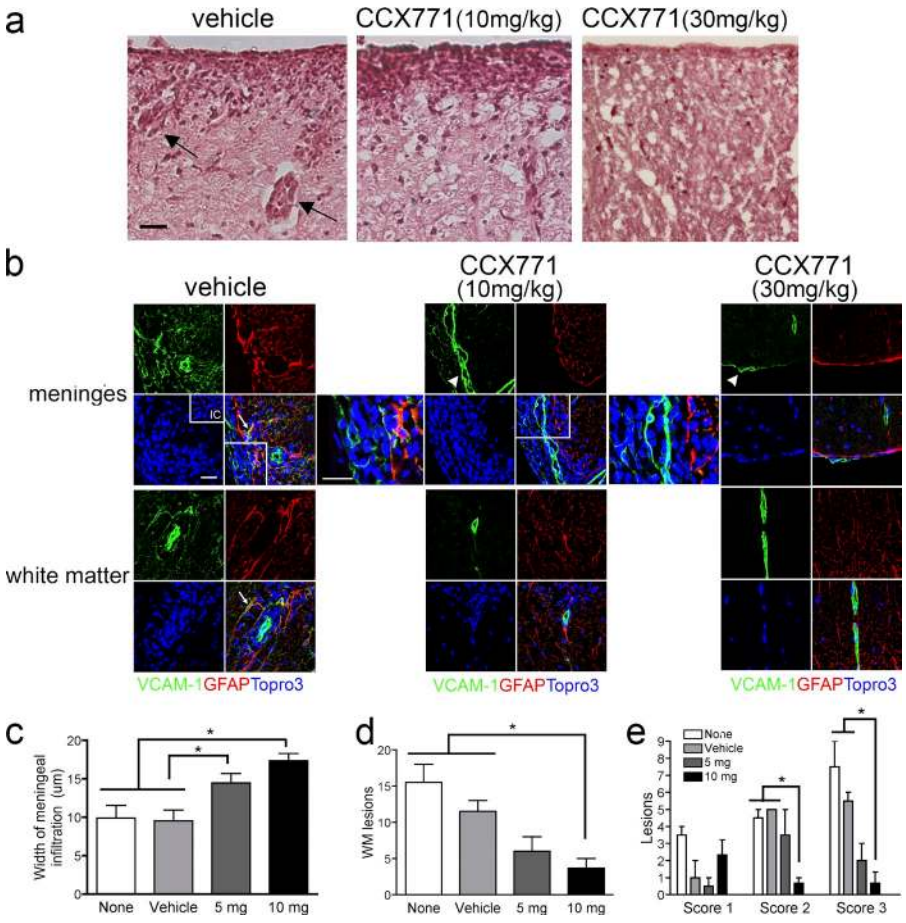

Figure 3. CXCR7 antagonism prevents leukocyte entry at the microvasculature. (a) Histological analyses of spinal cord tissues from vehicle- and CCX771-treated (10 or 30 mg/kg) mice 12 d after MOG-specific $CD4^+$ T cell transfer. Note perivascular cuffs in vehicle treated tissue section (arrows). Bars, 25 µm. (b) IHC and confocal imaging detection of GFAP (red) and VCAM-1 (green) within meninges (top images) and white matter (bottom images) of animals with EAE treated with vehicle (left) versus CCX771 at 10 or 30 mg/kg. Nuclei were counterstained with ToPro3 (blue). (inset) Isotype control (IC). Higher magnification images of boxed areas on lower power images of meninges from mice treated with vehicle and 10 mg/kg CCX771 are provided to the right of merged images. Note the lack of astrocyte but not meningeal (arrowheads) expression of VCAM-1 in CCX771-treated tissues. Analyses were performed on spinal cords harvested from three animals per group at peak of disease. Bars, 25 µm. Quantitation of meningeal width (c), lesion number (d), and lesion characteristics (e) in mice from four treatment groups: none (white bars), vehicle (light gray bars), CCX771 at 5 mg/kg (dark gray bars), and 10 mg/kg (black bars). Scoring of perivascular cuffs: 1 = 2–6 cells; 2 = 6–11 cells; 3 > 11 cells. n = 5 mice/group; data expressed as mean width (millimeters; c), number of white matter (WM) lesions (d), or number of lesions of each score (e) ± SEM. *, $P < 0.05$.

perivascular cuffs of vehicle versus CCX771-treated mice with EAE revealed a dose-dependent decrease in the numbers of infiltrating $CD3^+$ ($P = 0.0158$, 10 mg/kg; $P = 0.0068$, 30 mg/kg), $CD11b^+$ ($P = 0.0124$, 10 mg/kg; $P = 0.0033$, 30 mg/kg), and $B220^+$ ($P < 0.0001$, 30 mg/kg) cells (Fig. 4, b and c). Consistent with this, the majority of TNF expression was detected primarily within the meninges in CCX771-treated mice, whereas vehicle-treated mice also exhibited TNF expression in the parenchyma (Fig. 4 d). Collectively, these data suggest that CXCR7 antagonism is associated with loss of parenchymal VCAM-1 expression, preventing inflammatory infiltration at the level of the microvasculature and leading to accumulation of mononuclear cells within the meninges.

To determine whether CXCR7 antagonism affected the percentages and overall numbers of mononuclear subsets within the spinal cord parenchyma, we performed flow cytometric analyses of cells isolated from spinal cord tissues of vehicle and CCX771-treated (10 mg/kg) mice at the peak of disease. CXCR7 antagonism led to a decrease in both the percentages and total cell numbers of infiltrating $CD4^+$, $CD11b^+$, and $B220^+$ cells (Fig. 4, e and f). Analysis of $CD45^+CD11b^+$ populations revealed significant decreases in both activated microglia ($CD45^{hi}CD11b^{low}$) and macrophages ($CD45^{hi}CD11b^{hi}$; Fig. 4 f). Vehicle-exposed versus CCX771-exposed MOG-specific T cell lines exhibited identical levels of proliferation and cytokine expression during antigen-specific reactivation in vitro (Fig. S3). Analysis of cytokine expression within the spinal cord tissues of vehicle versus CCX771-treated mice at the peak of disease revealed no differences in levels of T cell cytokines (Fig. S4 a), suggesting that T cells within both meningeal and parenchymal compartments express similar levels of proinflammatory cytokines. Collectively, these data indicate that CXCR7 antagonism ameliorates EAE by preventing the parenchymal entry of leukocytes specifically via effects at the CNS microvasculature and that this limits the overall trafficking and entry of leukocytes to the CNS.

T cell cytokines regulate internalization of CXCL12 by brain endothelial cells via CXCR7

Previous studies showed that T cell–derived IL-1β contributes to leukocyte CNS entry and disease severity during EAE via loss of abluminal CXCL12 at the BBB (McCandless et al., 2009). CXCL12 removal from cell surfaces may occur in mammalian systems via CXCR7-mediated trafficking to lysosomes for degradation (Luker et al., 2010). Thus, we wondered whether various T cell cytokines might contribute to leukocyte egress through alterations in the expression or sequestration of CXCL12, with the latter occurring via regulation of the expression and/or activity of CXCR7. To test this

directly, we evaluated brain endothelial cell responses to T cell cytokines relevant to altered BBB during CNS autoimmunity. Primary brain microvessel endothelial cells (BMECs) treated with various doses of IL-17, IL-1β, IFN-γ, and TNF were evaluated for expression of CXCL12, CXCR4, and CXCR7 and the lysosomal-associated membrane protein

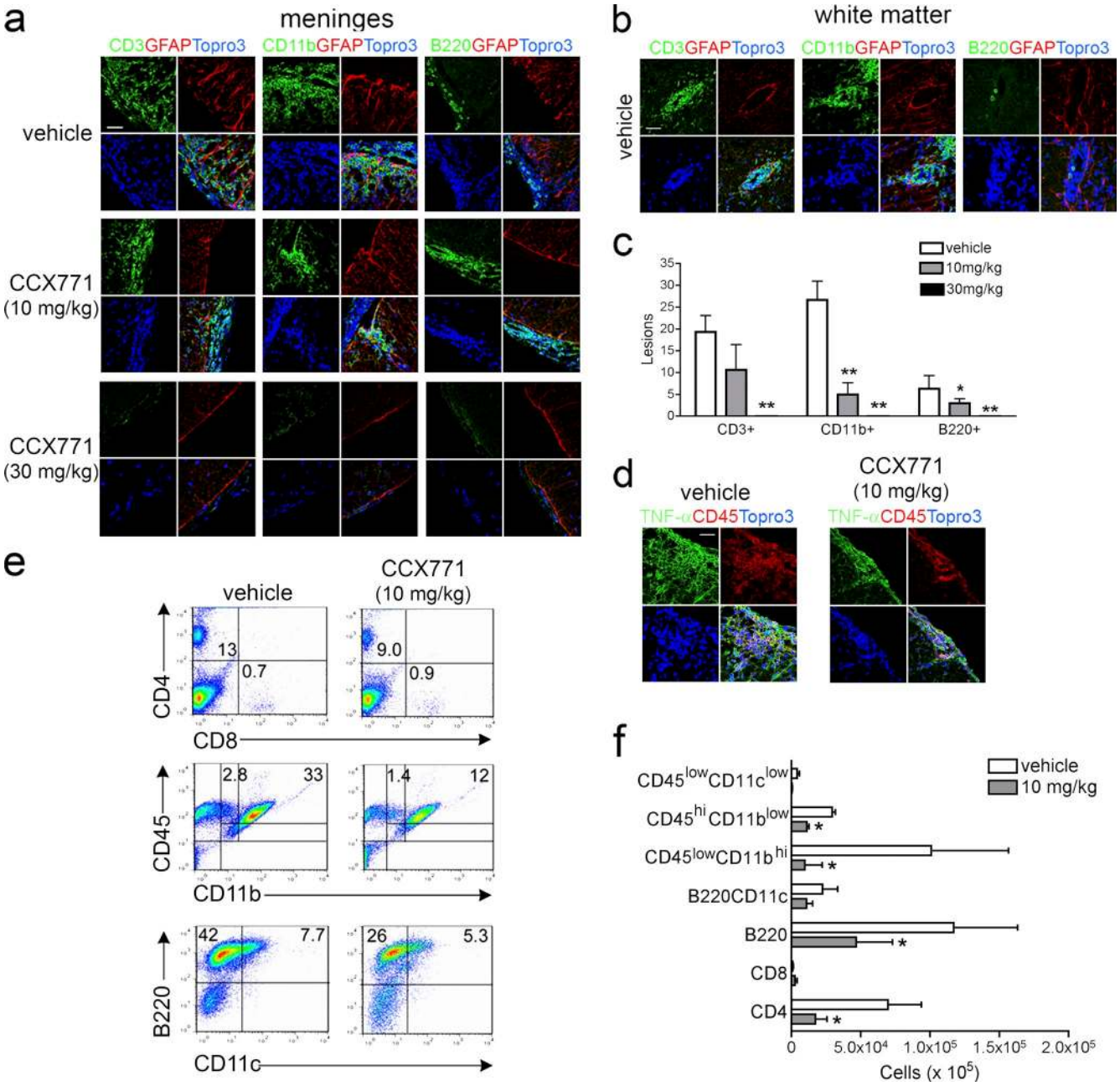

Figure 4. CXCR7 antagonism limits leukocyte trafficking to the CNS. IHC analyses of infiltrating leukocytes expressing CD3, CD11b, or B220 in respect to activated astrocytes (red, GFAP) within the meninges (a) and white matter (b) of vehicle-treated versus CCX771-treated (10 or 30 mg/kg) mice with EAE. Nuclei were counterstained with ToPro3 (blue). Bar, 10 µm. Analyses were performed on spinal cords harvested from three animals per group at peak of disease. (c) Quantitative analysis of numbers of white matter lesions attributed to the infiltration of $CD3^+$, $CD11b^+$, and $B220^+$ cells within spinal cord tissues of vehicle-treated and CCX771-treated (10 or 30 mg/kg) mice with EAE. Data are presented as the mean numbers of lesions in $n = 3$ mice per group ± SEM. (d) IHC analysis of infiltrating leukocytes (red, CD45) in respect to TNF expression (green) in spinal cords of vehicle-treated versus CCX771-treated (10 mg/kg) mice with EAE. Nuclei were counterstained with ToPro3 (blue). Bar, 25 µm. (e and f) Flow cytometric analysis of percentages (e, numbers in quadrants) and total cell numbers (f) of $CD4^+$, $CD8^+$, $CD45^+$, $CD11b^+$, $CD11c^+$, and $B220^+$ leukocytes harvested from spinal cords of vehicle-treated versus CCX771-treated (10 mg/kg) mice. Data depicting total cell numbers are presented as the mean numbers of cells derived from spinal cords of vehicle-treated versus CCX771-treated mice with EAE ± SEM from three experiments with five mice per group. *, $P < 0.05$; **, $P < 0.01$.

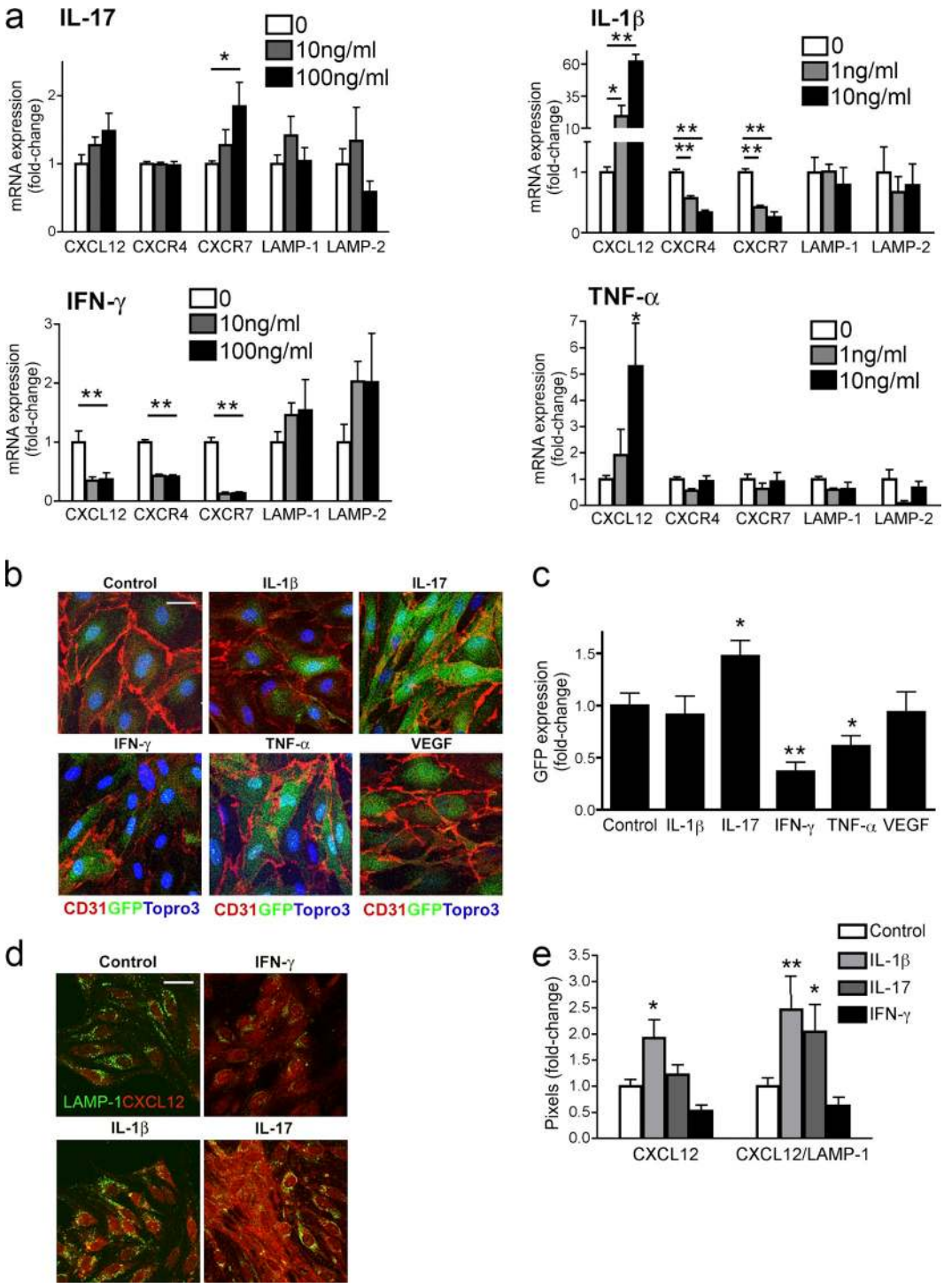

Figure 5. CXCR7 expression and CXCL12 internalization are altered by T cell cytokines. (a) Primary BMECs were treated with indicated doses of IL-17, IL-1β, IFN-γ, and TNF, and expression of CXCL12, CXCR4, CXCR7, LAMP-1, and LAMP-2 mRNA were measured via QPCR. Data from three experiments with triplicates are presented as the mean fold change in mRNA levels over untreated controls ± SEM. *, $P < 0.05$; **, $P < 0.001$. (b) BMECs derived from CXCR7$^{GFP/+}$ mice were treated with cytokines (IL-1β, IL-17, IFN-γ, and TNF) or VEGF (100 ng/ml) or left untreated (control), and CD31 (red) and GFP (green) expression was evaluated. Nuclei counterstained with ToPro3 (blue). Bar, 10 µm. (c) Quantitative analysis of GFP expression in cytokine- or VEGF-treated CD31$^+$ CXCR7$^{GFP/+}$BMECs. Data from three experiments performed in triplicate and presented as the mean fold change in GFP expression over untreated BMECs ± SEM. *, $P < 0.05$; **, $P < 0.001$. (d) LAMP-1 (green) and CXCL12 (red) colocalization in BMECs left untreated (control) or treated with IFN-γ, IL-1β, and IL-17. Bar, 10 µm. (e) Quantitation of CXCL12 and colocalization of CXCL12 and LAMP-1 staining in control and IL-1β–, IL-17–, and IFN-γ–treated BMECs. Data from three experiments in which five images were analyzed in each of three replicates per treatment group and presented as mean fold change over untreated controls. *, $P < 0.05$; **, $P < 0.001$.

(LAMP)-1 and LAMP-2, which are components and markers of the lysosomal membrane, via quantitative RT-PCR (QPCR; Fig. 5 a). IL-17 led to a significant increase in CXCR7 mRNA levels ($P = 0.025$), whereas both IL-1β and IFN-γ led to dose-dependent decreases in the mRNA levels of both CXCR4 and CXCR7 ($P < 0.01$ for all comparisons; Fig. 5 a, top and bottom). Similarly, BMECs derived from $CXCR7^{GFP/+}$ mice treated with high doses of cytokine and assessed for changes in GFP expression via quantitative confocal microscopic analysis exhibited significantly increased GFP expression after treatment with IL-17 ($P = 0.013$) and decreased GFP expression after treatment with IFN-γ ($P = 0.0003$; Fig. 5, b and c). In contrast with the QPCR results, levels of GFP expression were not affected by IL-1β, but were decreased by treatment with TNF ($P = 0.015$; Fig. 5, a–c). BMEC CXCL12 expression was significantly increased by treatment with either IL-1β ($P = 0.0006$) or TNF ($P = 0.005$; Fig. 5 a, right top and bottom), but was decreased by treatment with IFN-γ ($P = 0.019$; Fig. 5 a, bottom left). LAMP-1 and LAMP-2 mRNA levels were not significantly altered by cytokines (Fig. 5 a). Colocalization of CXCL12 and LAMP-1 within BMECs, as assessed by confocal IHC analysis, was significantly increased by treatment with IL-17 ($P = 0.014$) or IL-1β ($P = 0.0007$; Fig. 5, d and e), whereas treatment with IFN-γ decreased CXCL12 internalization.

To specifically analyze the sequestration of extracellular CXCL12, we evaluated cytokine-mediated uptake of exogenous fluorescent CXCL12-mCherry fusion protein via confocal IHC. This fusion protein exhibits CXCR4-binding kinetics and signaling comparable to unfused CXCL12 and has been used to quantify inhibition of CXCR7 binding by antagonists (Luker et al., 2009; Naumann et al., 2010). Exposure of BMECs to 300 ng/ml CXCL12-mCherry, but not mCherry alone, leads to colocalization of the fusion protein with LAMP-1 (Fig. 6 a). Analysis of BMECs treated with IL-1β ($P < 0.0001$) and IL-17 ($P < 0.0001$) revealed significant increases in CXCL12-mCherry internalization over those left untreated or treated with IFN-γ (Fig. 6, a and b). Internalization of CXCL12-mCherry in IL-1β–treated ($P = 0.002$) or IL-17–treated ($P = 0.016$) BMECs exhibited dose-dependent inhibition by CCX771 (Fig. 6 c), indicating that this process is mediated by CXCR7. Consistent with this, examination of CXCL12-mCherry internalization within lysosomes in BMECs exposed to a neutralizing, anti-CXCR4 antibody did not demonstrate a role for CXCR4 in this process (Fig. S4 b). Taken altogether, these data indicate that T cell cytokines regulate the levels of extracellular CXCL12 via effects on the expression of chemokine or on expression or activity of CXCR7.

Endothelial cell internalization of CXCL12 leads to its colocalization with CD31 in spinal cord postcapillary venules in mice with EAE induced by active immunization (McCandless et al., 2006), whereas mice with adoptive transfer EAE exhibit complete loss of CXCL12 at this site (Fig. S5 a). Use of $CXCR7^{GFP/+}$ mice to evaluate CXCL12 expression patterns revealed similar results as those observed using CD31 to identify vessels with abluminal CXCL12 observed in naive animals and lack of CXCL12 at sites of lesions in mice with adoptive transfer EAE (Fig. S5 b). Thus, to determine whether CXCR7 antagonism altered the BBB expression of CXCL12 in vivo, we analyzed the kinetics of CXCL12 removal at the CNS vasculature at various time-points posttransfer of encephalitogenic T cells. Similar amounts of abluminal CXCL12 around $CD31^+$ postcapillary venules was observed in the spinal cords of mice from both treatment groups at day 2 after transfer of MOG-specific T cells, but was completely absent by day 8 in mice treated with vehicle. Animals treated with CXCR7 antagonist (10 mg/kg) exhibited persistent abluminal CXCL12 until 10 d after transfer (Fig. 6, d and e). Analysis of panCXCL12 mRNA levels in IL-1β–treated BMECs exposed to vehicle versus CCX771 and CXCL12β (Stumm et al., 2002) mRNA levels in spinal cords derived from mice at peak clinical disease (day 10) revealed no effects of antagonist on CXCL12 expression (Fig. S6), suggesting that the increased CXCL12 protein observed during CXCR7 antagonism is caused by blockade of its internalization by CNS endothelium.

DISCUSSION

The current study provides compelling evidence that CXCR7-mediated internalization of CXCL12 is critical for the parenchymal infiltration of autoreactive leukocytes during CNS autoimmunity and that IL-17, IFN-γ, and IL-1β regulate this process via alterations in CNS endothelial cell expression of CXCL12 and CXCR7. This is supported by both in vitro and in vivo experiments in which CXCR7 antagonism prevented the endothelial cell internalization and lysosomal delivery of CXCL12, leading to increased extracellular levels of the chemokine. In vitro, endothelial cell internalization of CXCL12 was augmented by treatment with IL-17 and IL-1β, decreased by IFN-γ, and completely blocked by CXCR7 antagonism. In vivo, endothelial cell CXCR7, which was detected exclusively at post-capillary venules within murine CNS tissues, exhibited increased expression at this location in specimens derived from mice with EAE induced by the adoptive transfer of MOG-specific T cells. Most strikingly, administration of a CXCR7 antagonist during induction of EAE led to a dose-dependent inhibition of disease severity and promotion of recovery and complete amelioration of symptoms when administered to mice during ongoing disease. The in vivo effect of CXCR7 antagonism during EAE was associated with inhibition of leukocyte trafficking from leptomeningeal vessels to the microvasculature, leading to a significant widening of meningeal infiltrates and a significant decrease in the numbers and extents of parenchymal infiltrates. This latter effect of CXCR7 antagonism was also associated with a complete loss of VCAM-1 up-regulation by spinal cord astrocytes, an essential step in the parenchymal entry of leukocytes during EAE (Gimenez et al., 2004). These are the first in vivo data demonstrating a role for CXCR7-mediated internalization of CXCL12 in an autoimmune disease, identifying the receptor as a putative therapeutic target for MS.

Several studies suggest that CXCR7 primarily functions to internalize CXCL12 to efficiently transduce changes in chemokine gene expression, and thereby stringently regulate CXCR4 signaling. Although this function has been well characterized during zebrafish development (Valentin et al., 2007; Boldajipour et al., 2008), recent in vitro studies suggest CXCR7 also sequesters CXCL12 in mammals (Luker et al., 2010; Naumann et al., 2010). Consistent with this function, CXCR7 cycles continuously between the cell surface and endosomal compartments and is rapidly replenished from intracellular stores after ligand-induced internalization (Naumann et al., 2010). In the normal adult brain, CXCR7 mRNA is expressed by neurons and endothelial cells (Schönemeier et al., 2008a). Although factors that regulate CXCR7 mRNA expression within the CNS endothelium are unknown, they are likely to involve inflammatory pathways, as permanent

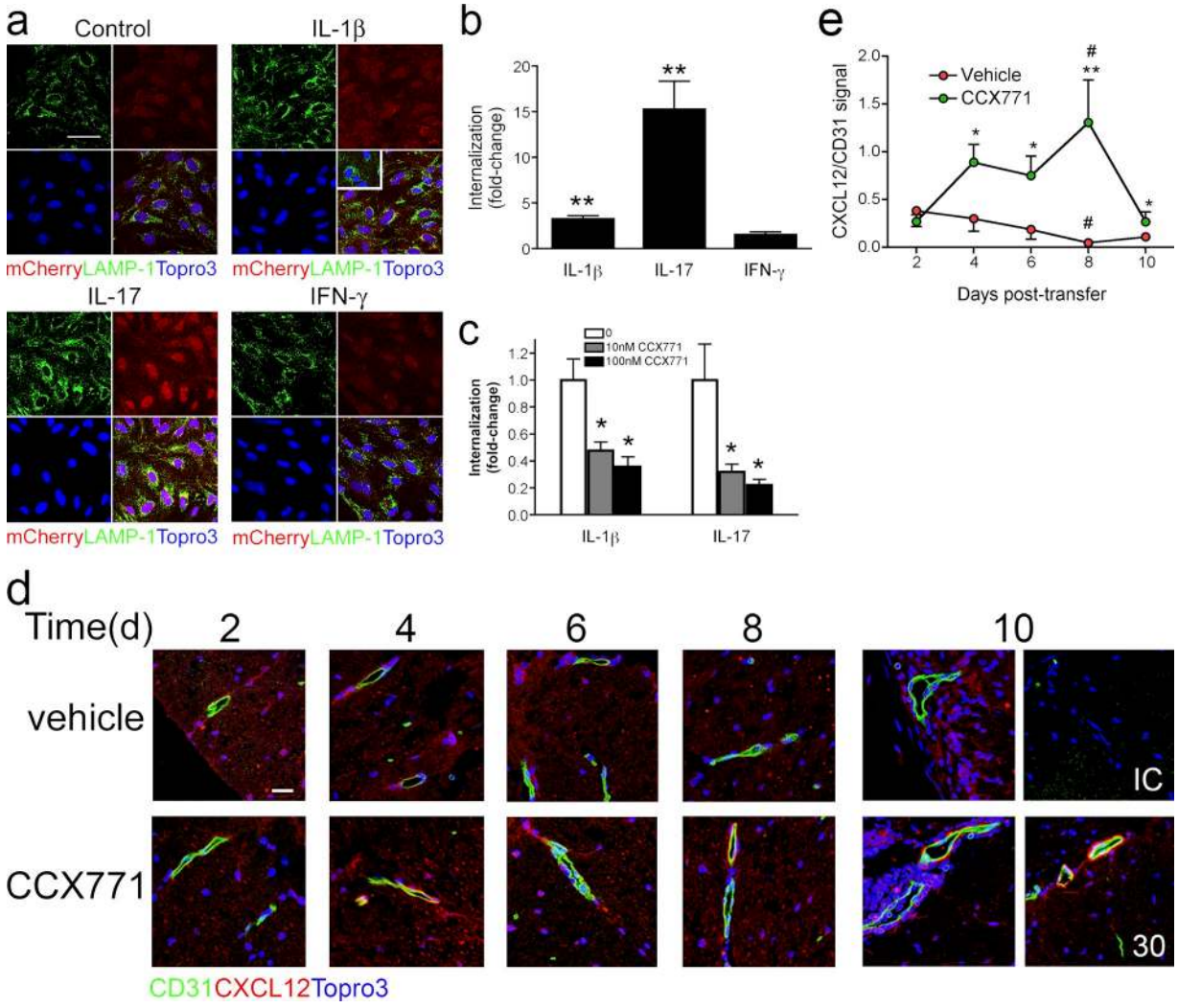

Figure 6. BMEC internalization of CXCL12 is mediated by CXCR7. (a) BMECs were left untreated (control) or treated overnight with IL-1β (10 ng/ml), IL-17 (100 ng/ml), or IFN-γ (100 ng/ml) and internalization of CXCL12-Cherry (red, L12mCherry; left) versus mCherry alone (inset) via colocalization with LAMP-1 (green). Nuclei were counterstained with ToPro3 (blue) Magnification 40×. Bar, 20 µm. (b) Fold changes in internalization of CXCL12-Cherry in BMECs treated with IL-1β (10 ng/ml), IL-17 (100 ng/ml), or IFN-γ (100 ng/ml) over those left untreated. (c) Fold changes in internalization of CXCL12-Cherry in IL-1β– and IL-17–treated BMECs left unexposed or exposed to 10 nM or 100 nM (filled bars) CCX771. All quantitative data are presented as mean ± SEM for an experiment done in triplicate, and are representative of three to four experiments. **, $P < 0.001$; *, $P < 0.05$. (d) Detection of CD31 (green) and CXCL12 (red) within spinal cords of mice treated with vehicle or CCX771 (10 mg/kg for all bottom panels except for the far right panel, which is from a mouse treated with 30 mg/kg) at 2, 4, 6, 8, and 10 d after transfer of MOG-specific $CD4^+$ T cells. Nuclei have been counterstained with Topro3 (blue). Bar, 20 µm. IC, isotype control. Data are representative of 10 images each from 3 mice per treatment group per time point. (e) Quantitative analysis of CXCL12 expression on $CD31^+$ venules within the spinal cords of mice at various days after transfer of MOG-specific T cells. Data derived from venules analyzed within four to eight images per spinal cord for three mice per treatment group for each time point, and are expressed as the mean ratios of signal intensity of CXCL12/CD31 ± SEM. **, $P < 0.001$ and *, $P < 0.05$ for comparisons between treatment groups on the same day after transfer; #, $P < 0.05$ for comparisons between days 2 and 8 after transfer within a treatment group.

middle cerebral artery occlusion leads to increased CXCR7 mRNA within vascular elements of the ipsilateral cortex (Schönemeier et al., 2008b). Consistent with this, we observed increased levels of expression of CXCR7 along the microvasculature during EAE and after in vitro treatment of BMECs with IL-17, a T cell cytokine implicated in the trafficking of immune cells into the CNS parenchyma (Kebir et al., 2007; Fabis et al., 2008; Huppert et al., 2010). IL-17 and IL-1β, another cytokine implicated in T cell entry early in the course of EAE (Sutton et al., 2006), also promoted the internalization of CXCL12 and its colocalization with LAMP-1 within BMECs, supporting the notion that proinflammatory cytokines regulate localizing molecules at the BBB. IFN-γ, however, decreased BMEC expression of CXCL12, CXCR4, and CXCR7. These results are consistent with prior reports that IFN-γ down-regulates CXCR4 in neutrophils and the homeostatic chemokines CXCL13 and CCL21 in lymphoid tissues (Nagase et al., 2002; Mueller et al., 2007). Thus, although CXCR7 and CXCL12 likely exist in equilibrium under homeostatic conditions, preserving localizing cues that slow leukocyte egress into the parenchyma, inflammatory cytokines may differentially shift this equilibrium in favor of preventing or promoting leukocyte entry.

Studies examining the role of T cell cytokines in the location of inflammatory lesions during EAE have determined that IL-17 is also essential for brainstem inflammation (Kroenke et al., 2010). In our study, levels of CXCR7 in all white matter regions were similar in naive mice whereas mice with EAE exhibited significant increases in CXCR7 expression in spinal cord and cerebellum. In contrast, levels of CXCR7 expression remained unchanged from baseline with the brainstem, a CNS region that typically does not develop any inflammatory lesions in classical EAE models. Of interest, transfer of MOG-specific T cells that express high levels of IL-17 induce more brain inflammation and atypical EAE (Stromnes et al., 2008). Our data demonstrating that high levels of IL-17 induce CXCR7 expression in BMECs suggest that this cytokine may differentially affect leukocyte entry in various CNS regions through effects on CXCR7-mediated internalization of CXCL12 at the microvasculature. Further studies using tissue-specific transgenic approaches are planned to further define the in vivo effects of Th17 cells on CXCR7, CXCR4, and CXCL12 location and activity at the BBB during EAE. Although we did not detect CXCR7 expression by infiltrating leukocytes within the CNS, we did identify a subpopulation of $CD19^+$ cells that expressed CXCR7 within lymphoid tissues in MOG-immunized animals. Thus, CXCR7 may play a role in the early adaptive immune responses of B cells, as suggested by a previous study (Infantino et al., 2006).

Infiltrating, autoreactive leukocytes require binding of integrin α4β1 (VLA-4) to VCAM-1 for entry into CNS parenchyma (Yednock et al., 1992; Baron et al., 1993). The success of natalizumab, a humanized monoclonal antibody against α4-integrin, in preventing new lesion formation in MS patients (Belachew et al., 2011) indicates that targeting molecules involved in leukocyte entry is indeed a tractable approach for the development of novel therapies for this disease. However, the targeting of molecules expressed by immune cells may not be specific for the CNS, as natalizumab also targets gastrointestinal-homing lymphocytes (Baron et al., 1993). In addition, natalizumab treatment is associated with progressive multifocal leukoencephalopathy (PML), an opportunistic, fatal encephalitis caused by JC virus (Clifford, 2008). Our data indicate that targeting CXCR7 specifically inhibits lymphocyte entry into the CNS via effects on the CNS microvasculature in both the meningeal and parenchymal compartments. The lack of inflammation at high doses of CCX771 suggests that CXCR7 is required for entry of cells into the meningeal compartment, which is the first site of leukocyte accumulation during neuroinflammation. Thus, low-dose CCX771 partially blocked leukocyte recruitment, allowing meningeal accumulation, whereas high-dose CCX771 completely abrogated leukocyte localization at both sites. In addition, CXCR7 antagonism prevented lymphocyte egress via persistent BBB expression of CXCL12, effectively diminishing parenchymal responses to T cell cytokines, such as TNF, which are required for astrocyte expression of VCAM-1 (Gimenez et al., 2004). Studies examining CXCR7 antagonism in the contexts of acute and chronic CNS infections will reveal additional insights regarding the safety of this approach.

In summary, our study provides evidence that CXCR7-mediated sequestration of CXCL12 at the CNS vasculature regulates leukocyte localization at this site during CNS autoimmunity. We also provide evidence that the differential responses of CNS regions to varying ratios of Th1 versus Th17 cells during induction of autoimmunity may be caused by opposing effects of IFN-γ and IL-17 on BBB CXCR7 expression. Thus, the ubiquitous expression of CXCR7 at CNS postcapillary venules may provide a molecular switch that preserves or destroys barriers to leukocyte entry, depending on the cytokine milieu. Targeting CXCR7 may therefore provide additional specificity for the prevention of lymphocyte egress regardless of the cytokine profile associated with disease expression (Axtell et al., 2010).

MATERIALS AND METHODS

Animals and antibodies. C57BL/6 (The Jackson Laboratory) and $CXCR7^{GFP/+}$ mice were maintained in pathogen-free conditions (Department of Comparative Medicine, Washington University, St. Louis, MO), and studies were performed in compliance with the guidelines of the Washington University School of Medicine Animal Safety Committee. Antibodies used include CXCL12 rabbit polyclonal (PeproTech), actin antibodies (Sigma-Aldrich), IgG isotype (Jackson ImmunoResearch Laboratories), monoclonal rat anti–mouse-CD31, CD11b, Thy1.1, VCAM-1 (BD), anti-CD3 (Dako), anti-B220 (R&D Systems), GFAP (Zymed), LAMP-1 (US Biologicals), GFP (Invitrogen), and fluorescently conjugated antibodies against CD4, CD8, CD19, CD11b, CD11c, B220, and CD45 (BD).

Generation of CXCR7 knock-in mice. The entire open reading frame of *Cxcr7* gene encoded by exon 2 was replaced by EGFP sequence. A 5′ homology arm containing a 5.4-kb genomic fragment containing part of intron 1 and 26 bp of exon 2 immediately upstream of the ATG start codon was PCR amplified using C57BL/6 genomic DNA as templates, and then cloned in front of EGFP coding sequence. A 3′ homology arm containing a 5.2-kb

genomic fragment including DNA sequence immediately downstream of stop codon of *Cxcr7* gene was PCR amplified using C57BL/6 genomic DNA and cloned after a neomycin-resistant gene cassette flanked by Lox P sites. The sequence of the targeting construct was confirmed by DNA sequencing. The targeting construct was linearized by Not I restriction enzyme and electroporated into albino C57BL/6 embryonic stem (ES) cells. The colonies doubly resistant for the aminoglycoside G418 and ganciclovir were screened by Southern blot analyses with BsrgI, BamHI, and HindIII digestions for homologous recombination. Positive clones were injected into mouse blastocysts. Mice were subsequently crossed with EIIa-cre to remove the neomycin-resistant cassette.

Analysis of CCX771 selectivity. Human neutrophils were isolated from whole blood and lymphocytes from buffy coats (Stanford Blood Center, Stanford, CA) via Ficoll-Paque PLUS centrifugation followed by red blood cell lysis. Lymphocyte fractions were activated in vitro, as previously described (Walters et al., 2010). CEM, Molt-4, and U937 cells were obtained from American Type Culture Collection (ATCC) and cultured in RPMI-1640 medium (Sigma-Aldrich) supplemented with 10% FBS. U937 cells were additionally treated with dibutyryl cyclic-AMP (Sigma-Aldrich). Baf3 and L1.2 cells (ATCC) were stably transfected with human CCR5 and ChemR23, respectively, and were cultured in RPMI-1640 medium/10% FBS supplemented with murine IL-3. Chemokines were purchased from R&D Systems. Calcium flux, chemotaxis, and radioligand binding assays were all performed as previously described (Zabel et al., 2009; Walters et al., 2010). Analysis of CCX771 activity against a panel of G protein–coupled receptors (GPCRs; Table S2) was conducted under contract by Cerep using the Non-Peptide Receptor Express Profile option (http://www.cerep.fr/cerep/users/pages/downloads/pharmacology.asp).

Assessment of plasma concentrations of CCX771. A total of 12 male BALB/c mice (The Jackson Laboratory) were administered a subcutaneous injection of 10 mg/kg CCX771, formulated as a solution in 10% Captisol with dosing volume at 1 ml/kg. Plasma samples were obtained from retro-orbital obtained blood (100 μl) collected into EDTA tubes at determined time points. Each animal was bled only twice during the study; thus, each time-point reflects data from three of the animals on study. After protein precipitation, the supernatant solutions were analyzed by HPLC-MS/MS using a validated method (nominal plasma concentration; range from 1 to 1,000 ng/ml). Pharmacokinetic values for CCX771 were generated using noncompartmental analysis with WinNonlin Professional version 5.2 (Pharsight).

EAE induction and in vivo treatment with CCX771. Active EAE was induced in 8–12-wk-old female C57BL/6 (The Jackson Laboratory) mice by subcutaneous immunization with murine myelin oligodendroglial glycoprotein peptide 35–55 (MOG; Sigma-Aldrich) and followed for clinical disease as previously described. MOG-specific T cells were generated as previously described (Gimenez et al., 2004). Activated cells were collected and transferred retroorbitally at 10^7 cells per mouse. Mice from all experiments were graded for clinical manifestations of EAE by the following criteria: 1, tail weakness; 2, difficulty righting; 3, hindlimb paralysis; 4, forelimb weakness or paralysis; 5, moribund or dead. CCX771 (ChemoCentryx) or vehicle (10% Captisol) was administered daily to mice subcutaneously at doses of 5, 10, or 30 mg/kg in 100 ml of vehicle at the time of adoptive transfer of T cells or when mice achieved a clinical score of 1.

LFB staining of spinal cord. Frozen sections were stained for myelin using 0.1% LFB and counter stained with 0.1% cresyl violet. The sections were differentiated with 0.5% lithium carbonate, counterstained with cresyl violet for 20 min, and mounted for imaging using an Axioskop 40 light microscope (Carl Zeiss, Inc.).

Assays of T cell proliferation and cytokine expression. MOG-specific T cell lines underwent three 7-d rounds of restimulation in the presence of irradiated splenocytes (ratio 1:5), 0.01 mg/ml MOG_{p35-55}, and IL-2, IL-12, and anti-IL-4, as previously described (Gimenez et al., 2006). During the third restimulation, T cells were treated for 4 d with various doses of CCX771 (ChemoCentryx) versus vehicle (DMSO) or CCX704, an inactive CXCR7 antagonist, and then evaluated for proliferation and cytokine expression. For proliferation responses, T cells were preloaded with CFSE (Invitrogen) before third restimulation. For cytokine responses, supernatants of restimulated cells were evaluated for Th1/Th2/Th17 cytokine expression via cytokine bead array (BD). Data acquisition for CFSE labeling and cytokine expression panel was performed via BD FACSCalibur flow cytometry and analyzed by BD FCAP Array software.

QPCR analysis of spinal cord expression. Total RNA was prepared and QPCR was performed as previously described (Klein et al., 2005) using primers for TNF, IFN-γ, IL-10, IL-17, and IL-1β, whose sequences have been previously published (Klein et al., 2004, 2005).

Preparation of murine BMECs. Murine BMECs were generated using previously described methods (Perrière et al., 2005), with slight modifications. In brief, cortices of 8-wk-old C57BL/6J mice were dissected free of meninges, minced, and digested with 1 mg/ml collagenase CLS2 (Worthington) and 30 U/ml DNase (Sigma-Aldrich) at 37°C for 45 min, with shaking. The digested cell pellet was separated by centrifugation in 20% BSA in DME (1,000 *g* for 20 min), followed by a further digestion in 1 mg/ml collagenase-dispase (Roche) and 10 U/ml DNase at 37°C for 30 min, with shaking. Microvessel fragments were subsequently isolated on a 33% continuous Percoll gradient (1,000 *g* for 10 min), washed twice with DME, and plated to T-25 flasks coated with 0.1 mg/ml mouse collagen type IV and 0.1 mg/ml human fibronectin.

BMEC expression of CXCR7. Primary BMECs were treated with various concentrations of IL-17, IL-1β, TNF, and IFN-γ or left untreated for 24 h before undergoing total RNA isolation, as previously described (McCandless et al., 2006). QPCR analysis of CXCR7 was accomplished using a Taqman gene expression assay kit (Applied Biosystems), which uses the FAM/TAMRA reporter with primers spanning the first and second exon and amplifies a 77-bp product. Calculated copies were normalized against copies of the housekeeping gene GAPDH.

Histological, IHC, and immunocytochemical analyses. Murine CNS tissues were isolated and frozen sections were permeabilized, blocked, and stained as previously described (McCandless et al., 2006). Histological analyses, including myelin staining and IHC detection of CD31, CXCL12, VCAM-1, TNF, GFAP, CD3, and CD11b with nuclear ToPro3 counterstaining, were performed as previously described (Gimenez et al., 2004; McCandless et al., 2008b).

Colocalization of CXCL12 and LAMP-1 within primary BMECs was performed after fixation with 4% paraformaldehyde for 10 min and permeabilization with block in 0.1% Triton X-100 and 10% goat serum for 30 min at room temperature. BMECs were incubated with the primary antibodies rabbit anti–human CXCL12 (PeproTech, 1:20) and rat anti–mouse LAMP-1 (1:50; US Biologicals) in blocking buffer for 20 min at room temperature. Cells were washed three times in PBS, and then incubated in fluorescently conjugated goat anti–rabbit Alexa Fluor 555 and goat anti–rat Alexa Fluor 488 (1:1,000; Invitrogen) secondary antibodies in blocking buffer for 15 min at room temperature. Cells were washed, counterstained with ToPro3, and coverslipped before being visualized on the confocal microscope and accompanying software.

Flow cytometry. Cells were isolated from the draining lymph nodes, spleens, and spinal cords of MOG-immunized $CXCR7^{GFP/+}$ or C57BL/6 mice at 9 d after immunization and stained with fluorescently conjugated antibodies to CD4, CD8, CD19, CD11b, CD11c, and CD45 as previously described (McCandless et al., 2006). Removal of spinal cords was accomplished

via pressure-syringing using an 18 gauge needle. Data collection and analysis were conducted using a FACSCalibur flow cytometer using CellQuest software (BD), as previously described (McCandless et al., 2009).

Generation of mCherryCXCL12 and internalization experiments. mCherry plasmid DNA was used to transfect 293T cells as previously described (Luker et al., 2009). Supernatants containing mCherry-CXCL12 were collected 24 h after transfection. To assess mCherry CXCL12 uptake, BMECs were treated with IL-17 (100 ng/ml), IL-1β (10 ng/ml), IFN-γ (100 ng/ml) or control media for 24 h in media containing vehicle, CXCR7 antagonist, CCX771, or anti-CXCR4 antibody (R&D Systems). BMECs were incubated for 2 h with mCherry-CXCL12 supernatants, and then fixed with ice-cold methanol for 10 min. Cells were then counterstained with ToPro3 and visualized immediately, or further stained with LAMP-1 as described in Histological, IHC, and immunocytochemical analyses.

Statistical analyses. All values are expressed as mean ± SEM. Student's *t* test was used to determine the statistical significance of QPCR and histological and flow cytometry analyses. Mean maximal disease severity significance was determined by the Mann-Whitney nonparametric test, with values of $P < 0.05$ considered statistically significant for all analyses. Statistical significance of disease severity curves, effects of cytokines on CXCR7 expression, and activity in BMECs and in vivo CXCL12 internalization was determined using one-way Analysis of Variance (ANOVA) with Bonferroni's multiple comparison test.

Online supplemental material. Fig. S1 depicts the generation of CXCR7 GFP knock-in mice. Fig. S2 shows that CXCR7 antagonism prevents demyelination during EAE. Fig. S3 shows that CXCR7 antagonism does not affect MOG-specific T cell reactivation. Fig. S4 shows cytokine levels within spinal cord parenchyma in mice treated with vehicle versus CXCR7 antagonist and that BMEC internalization of CXCL12 does not require CXCR4. Fig. S5 depicts abluminal CXCL12 at post-capillary venules during EAE induced by adoptive transfer of MOG-specific $CD4^+$ T cells and immunization with MOG. Fig. S6 shows that CXCR7 antagonism does not alter CXCL12 mRNA levels in BMECs or in spinal cords of mice with EAE.

The authors thank J. Sim for technical assistance.

This study was supported by National Institutes of Health (NIH)/National Institute of Neurological Disorders and Stroke grant NS059560 and National Multiple Sclerosis Society grant RG3982 (R.S. Klein) and by NIH grants R01CA136553, R01CA136829, and P50CA093990 (to G.D. Luker).

The authors have no conflicting financial interests.

Submitted: 23 September 2010
Accepted: 13 January 2011

REFERENCES

Abbott, N.J., L. Rönnbäck, and E. Hansson. 2006. Astrocyte-endothelial interactions at the blood-brain barrier. *Nat. Rev. Neurosci.* 7:41–53. doi:10.1038/nrn1824

Afonso, P.V., S. Ozden, M.C. Prevost, C. Schmitt, D. Seilhean, B. Weksler, P.O. Couraud, A. Gessain, I.A. Romero, and P.E. Ceccaldi. 2007. Human blood-brain barrier disruption by retroviral-infected lymphocytes: role of myosin light chain kinase in endothelial tight-junction disorganization. *J. Immunol.* 179:2576–2583.

Argaw, A.T., Y. Zhang, B.J. Snyder, M.L. Zhao, N. Kopp, S.C. Lee, C.S. Raine, C.F. Brosnan, and G.R. John. 2006. IL-1beta regulates blood-brain barrier permeability via reactivation of the hypoxia-angiogenesis program. *J. Immunol.* 177:5574–5584.

Axtell, R.C., B.A. de Jong, K. Boniface, L.F. van der Voort, R. Bhat, P. De Sarno, R. Naves, M. Han, F. Zhong, J.G. Castellanos, et al. 2010. T helper type 1 and 17 cells determine efficacy of interferon-beta in multiple sclerosis and experimental encephalomyelitis. *Nat. Med.* 16:406–412. doi:10.1038/nm.2110

Baron, J.L., J.A. Madri, N.H. Ruddle, G. Hashim, and C.A. Janeway Jr. 1993. Surface expression of alpha 4 integrin by CD4 T cells is required for their entry into brain parenchyma. *J. Exp. Med.* 177:57–68. doi:10.1084/jem.177.1.57

Bartholomäus, I., N. Kawakami, F. Odoardi, C. Schläger, D. Miljkovic, J.W. Ellwart, W.E. Klinkert, C. Flügel-Koch, T.B. Issekutz, H. Wekerle, and A. Flügel. 2009. Effector T cell interactions with meningeal vascular structures in nascent autoimmune CNS lesions. *Nature.* 462:94–98. doi:10.1038/nature08478

Belachew, S., R. Phan-Ba, E. Bartholomé, V. Delvaux, I. Hansen, P. Calay, K.E. Hafsi, G. Moonen, L. Tshibanda, and M. Vokaer. 2011. Natalizumab induces a rapid improvement of disability status and ambulation after failure of previous therapy in relapsing-remitting multiple sclerosis. *Eur. J. Neurol.* 18:240–245. doi:10.1111/j.1468-1331.2010.03112.x

Boldajipour, B., H. Mahabaleshwar, E. Kardash, M. Reichman-Fried, H. Blaser, S. Minina, D. Wilson, Q. Xu, and E. Raz. 2008. Control of chemokine-guided cell migration by ligand sequestration. *Cell.* 132:463–473. doi:10.1016/j.cell.2007.12.034

Burns, J.M., B.C. Summers, Y. Wang, A. Melikian, R. Berahovich, Z. Miao, M.E. Penfold, M.J. Sunshine, D.R. Littman, C.J. Kuo, et al. 2006. A novel chemokine receptor for SDF-1 and I-TAC involved in cell survival, cell adhesion, and tumor development. *J. Exp. Med.* 203:2201–2213. doi:10.1084/jem.20052144

Carbajal, K.S., C. Schaumburg, R. Strieter, J. Kane, and T.E. Lane. 2010. Migration of engrafted neural stem cells is mediated by CXCL12 signaling through CXCR4 in a viral model of multiple sclerosis. *Proc. Natl. Acad. Sci. USA.* 107:11068–11073. doi:10.1073/pnas.1006375107

Clifford, D.B. 2008. Natalizumab and PML: a risky business? *Gut.* 57:1347–1349. doi:10.1136/gut.2008.155770

Craigie, E.H. 1920. On the relative vasculatiry of various parts of the central nervous sytsem of the albino rat. *J. Comp. Neurol.* 31:429–464. doi:10.1002/cne.900310504

Fabis, M.J., T.W. Phares, R.B. Kean, H. Koprowski, and D.C. Hooper. 2008. Blood-brain barrier changes and cell invasion differ between therapeutic immune clearance of neurotrophic virus and CNS autoimmunity. *Proc. Natl. Acad. Sci. USA.* 105:15511–15516. doi:10.1073/pnas.0807656105

Frohman, E.M., M.K. Racke, and C.S. Raine. 2006. Multiple sclerosis—the plaque and its pathogenesis. *N. Engl. J. Med.* 354:942–955. doi:10.1056/NEJMra052130

Gimenez, M.A., J.E. Sim, and J.H. Russell. 2004. TNFR1-dependent VCAM-1 expression by astrocytes exposes the CNS to destructive inflammation. *J. Neuroimmunol.* 151:116–125. doi:10.1016/j.jneuroim.2004.02.012

Gimenez, M.A., J. Sim, A.S. Archambault, R.S. Klein, and J.H. Russell. 2006. A tumor necrosis factor receptor 1-dependent conversation between central nervous system-specific T cells and the central nervous system is required for inflammatory infiltration of the spinal cord. *Am. J. Pathol.* 168:1200–1209. doi:10.2353/ajpath.2006.050332

Huppert, J., D. Closhen, A. Croxford, R. White, P. Kulig, E. Pietrowski, I. Bechmann, B. Becher, H.J. Luhmann, A. Waisman, and C.R. Kuhlmann. 2010. Cellular mechanisms of IL-17-induced blood-brain barrier disruption. *FASEB J.* 24:1023–1034. doi:10.1096/fj.09-141978

Infantino, S., B. Moepps, and M. Thelen. 2006. Expression and regulation of the orphan receptor RDC1 and its putative ligand in human dendritic and B cells. *J. Immunol.* 176:2197–2207.

Kebir, H., K. Kreymborg, I. Ifergan, A. Dodelet-Devillers, R. Cayrol, M. Bernard, F. Giuliani, N. Arbour, B. Becher, and A. Prat. 2007. Human TH17 lymphocytes promote blood-brain barrier disruption and central nervous system inflammation. *Nat. Med.* 13:1173–1175. doi:10.1038/nm1651

Klein, R.S., L. Izikson, T. Means, H.D. Gibson, E. Lin, R.A. Sobel, H.L. Weiner, and A.D. Luster. 2004. IFN-inducible protein 10/CXC chemokine ligand 10-independent induction of experimental autoimmune encephalomyelitis. *J. Immunol.* 172:550–559.

Klein, R.S., E. Lin, B. Zhang, A.D. Luster, J. Tollett, M.A. Samuel, M. Engle, and M.S. Diamond. 2005. Neuronal CXCL10 directs CD8+ T-cell recruitment and control of West Nile virus encephalitis. *J. Virol.* 79:11457–11466. doi:10.1128/JVI.79.17.11457-11466.2005

Körner, H., D.S. Riminton, D.H. Strickland, F.A. Lemckert, J.D. Pollard, and J.D. Sedgwick. 1997. Critical points of tumor necrosis factor action in central nervous system autoimmune inflammation defined by gene targeting. *J. Exp. Med.* 186:1585–1590. doi:10.1084/jem.186.9.1585

Kroenke, M.A., S.W. Chensue, and B.M. Segal. 2010. EAE mediated by a non-IFN-γ/non-IL-17 pathway. *Eur. J. Immunol.* 40:2340–2348. doi:10.1002/eji.201040489

Lees, J.R., P.T. Golumbek, J. Sim, D. Dorsey, and J.H. Russell. 2008. Regional CNS responses to IFN-γ determine lesion localization patterns during EAE pathogenesis. *J. Exp. Med.* 205:2633–2642. doi:10.1084/jem.20080155

Libert, F., M. Parmentier, A. Lefort, J.E. Dumont, and G. Vassart. 1990. Complete nucleotide sequence of a putative G protein coupled receptor: RDC1. *Nucleic Acids Res.* 18:1917. doi:10.1093/nar/18.7.1917

Luker, K., M. Gupta, and G. Luker. 2009. Bioluminescent CXCL12 fusion protein for cellular studies of CXCR4 and CXCR7. *Biotechniques*. 47:625–632. doi:10.2144/000113126

Luker, K.E., J.M. Steele, L.A. Mihalko, P. Ray, and G.D. Luker. 2010. Constitutive and chemokine-dependent internalization and recycling of CXCR7 in breast cancer cells to degrade chemokine ligands. *Oncogene*. 29:4599–4610. doi:10.1038/onc.2010.212

Mahabaleshwar, H., B. Boldajipour, and E. Raz. 2008. Killing the messenger: The role of CXCR7 in regulating primordial germ cell migration. *Cell Adh. Migr.* 2:69–70. doi:10.4161/cam.2.2.6027

Man, S., E.E. Ubogu, and R.M. Ransohoff. 2007. Inflammatory cell migration into the central nervous system: a few new twists on an old tale. *Brain Pathol.* 17:243–250. doi:10.1111/j.1750-3639.2007.00067.x

McCandless, E.E., Q. Wang, B.M. Woerner, J.M. Harper, and R.S. Klein. 2006. CXCL12 limits inflammation by localizing mononuclear infiltrates to the perivascular space during experimental autoimmune encephalomyelitis. *J. Immunol.* 177:8053–8064.

McCandless, E.E., L. Piccio, B.M. Woerner, R.E. Schmidt, J.B. Rubin, A.H. Cross, and R.S. Klein. 2008a. Pathological expression of CXCL12 at the blood-brain barrier correlates with severity of multiple sclerosis. *Am. J. Pathol.* 172:799–808. doi:10.2353/ajpath.2008.070918

McCandless, E.E., B. Zhang, M.S. Diamond, and R.S. Klein. 2008b. CXCR4 antagonism increases T cell trafficking in the central nervous system and improves survival from West Nile virus encephalitis. *Proc. Natl. Acad. Sci. USA*. 105:11270–11275. doi:10.1073/pnas.0800898105

McCandless, E.E., M. Budde, J.R. Lees, D. Dorsey, E. Lyng, and R.S. Klein. 2009. IL-1R signaling within the central nervous system regulates CXCL12 expression at the blood-brain barrier and disease severity during experimental autoimmune encephalomyelitis. *J. Immunol.* 183:613–620. doi:10.4049/jimmunol.0802258

McFarland, H.F., and R. Martin. 2007. Multiple sclerosis: a complicated picture of autoimmunity. *Nat. Immunol.* 8:913–919. doi:10.1038/ni1507

Mueller, S.N., K.A. Hosiawa-Meagher, B.T. Konieczny, B.M. Sullivan, M.F. Bachmann, R.M. Locksley, R. Ahmed, and M. Matloubian. 2007. Regulation of homeostatic chemokine expression and cell trafficking during immune responses. *Science*. 317:670–674. doi:10.1126/science.1144830

Nagase, H., M. Miyamasu, M. Yamaguchi, M. Imanishi, N.H. Tsuno, K. Matsushima, K. Yamamoto, Y. Morita, and K. Hirai. 2002. Cytokine-mediated regulation of CXCR4 expression in human neutrophils. *J. Leukoc. Biol.* 71:711–717.

Naumann, U., E. Cameroni, M. Pruenster, H. Mahabaleshwar, E. Raz, H.G. Zerwes, A. Rot, and M. Thelen. 2010. CXCR7 functions as a scavenger for CXCL12 and CXCL11. *PLoS One*. 5:e9175. doi:10.1371/journal.pone.0009175

Perrière, N., P. Demeuse, E. Garcia, A. Regina, M. Debray, J.P. Andreux, P. Couvreur, J.M. Scherrmann, J. Temsamani, P.O. Couraud, et al. 2005. Puromycin-based purification of rat brain capillary endothelial cell cultures. Effect on the expression of blood-brain barrier-specific properties. *J. Neurochem.* 93:279–289. doi:10.1111/j.1471-4159.2004.03020.x

Rajagopal, S., J. Kim, S. Ahn, S. Craig, C.M. Lam, N.P. Gerard, C. Gerard, and R.J. Lefkowitz. 2010. Beta-arrestin- but not G protein-mediated signaling by the "decoy" receptor CXCR7. *Proc. Natl. Acad. Sci. USA*. 107:628–632. doi:10.1073/pnas.0912852107

Schönemeier, B., A. Kolodziej, S. Schulz, S. Jacobs, V. Hoellt, and R. Stumm. 2008a. Regional and cellular localization of the CXCl12/SDF-1 chemokine receptor CXCR7 in the developing and adult rat brain. *J. Comp. Neurol.* 510:207–220. doi:10.1002/cne.21780

Schönemeier, B., S. Schulz, V. Hoellt, and R. Stumm. 2008b. Enhanced expression of the CXCl12/SDF-1 chemokine receptor CXCR7 after cerebral ischemia in the rat brain. *J. Neuroimmunol.* 198:39–45. doi:10.1016/j.jneuroim.2008.04.010

Sierro, F., C. Biben, L. Martínez-Muñoz, M. Mellado, R.M. Ransohoff, M. Li, B. Woehl, H. Leung, J. Groom, M. Batten, et al. 2007. Disrupted cardiac development but normal hematopoiesis in mice deficient in the second CXCL12/SDF-1 receptor, CXCR7. *Proc. Natl. Acad. Sci. USA*. 104:14759–14764. doi:10.1073/pnas.0702229104

Stromnes, I.M., L.M. Cerretti, D. Liggitt, R.A. Harris, and J.M. Goverman. 2008. Differential regulation of central nervous system autoimmunity by T(H)1 and T(H)17 cells. *Nat. Med.* 14:337–342. doi:10.1038/nm1715

Stumm, R.K., J. Rummel, V. Junker, C. Culmsee, M. Pfeiffer, J. Krieglstein, V. Höllt, and S. Schulz. 2002. A dual role for the SDF-1/CXCR4 chemokine receptor system in adult brain: isoform-selective regulation of SDF-1 expression modulates CXCR4-dependent neuronal plasticity and cerebral leukocyte recruitment after focal ischemia. *J. Neurosci.* 22:5865–5878.

Sutton, C., C. Brereton, B. Keogh, K.H. Mills, and E.C. Lavelle. 2006. A crucial role for interleukin (IL)-1 in the induction of IL-17–producing T cells that mediate autoimmune encephalomyelitis. *J. Exp. Med.* 203:1685–1691. doi:10.1084/jem.20060285

Vajkoczy, P., M. Laschinger, and B. Engelhardt. 2001. Alpha4-integrin-VCAM-1 binding mediates G protein-independent capture of encephalitogenic T cell blasts to CNS white matter microvessels. *J. Clin. Invest.* 108:557–565.

Valentin, G., P. Haas, and D. Gilmour. 2007. The chemokine SDF1a coordinates tissue migration through the spatially restricted activation of Cxcr7 and Cxcr4b. *Curr. Biol.* 17:1026–1031. doi:10.1016/j.cub.2007.05.020

Walters, M.J., Y. Wang, N. Lai, T. Baumgart, B.N. Zhao, D.J. Dairaghi, P. Bekker, L.S. Ertl, M.E. Penfold, J.C. Jaen, et al. 2010. Characterization of CCX282-B, an orally bioavailable antagonist of the CCR9 chemokine receptor, for treatment of inflammatory bowel disease. *J. Pharmacol. Exp. Ther.* 335:61–69. doi:10.1124/jpet.110.169714

Yednock, T.A., C. Cannon, L.C. Fritz, F. Sanchez-Madrid, L. Steinman, and N. Karin. 1992. Prevention of experimental autoimmune encephalomyelitis by antibodies against alpha 4 beta 1 integrin. *Nature*. 356:63–66. doi:10.1038/356063a0

Zabel, B.A., Y. Wang, S. Lewén, R.D. Berahovich, M.E. Penfold, P. Zhang, J. Powers, B.C. Summers, Z. Miao, B. Zhao, et al. 2009. Elucidation of CXCR7-mediated signaling events and inhibition of CXCR4-mediated tumor cell transendothelial migration by CXCR7 ligands. *J. Immunol.* 183:3204–3211. doi:10.4049/jimmunol.0900269